Technical Reference on Hydrogen Compatibility of Materials

Low-Alloy Ferritic Steels:
Tempered Fe-Ni-Cr-Mo Alloys (code 1212)

Prepared by:
B.P. Somerday, Sandia National Laboratories

Editors
C. San Marchi
B.P. Somerday
Sandia National Laboratories

This report may be updated and revised periodically in response to the needs of the technical community; up-to-date versions can be requested from the editors at the address given below or downloaded at http://www.ca.sandia.gov/matlsTechRef/ . The success of this reference depends upon feedback from the technical community; please forward your comments, suggestions, criticisms and relevant public-domain data to:

Sandia National Laboratories
Matls Tech Ref
B.P. Somerday (MS-9402)
7011 East Ave
Livermore CA 94550.

This document was prepared with financial support from the Safety, Codes and Standards program element of the Hydrogen, Fuel Cells and Infrastructure program, Office of Energy Efficiency and Renewable Energy; Pat Davis is the manager of this program element. Sandia is a multiprogram laboratory operated by Sandia Corporation, a Lockheed Martin Company, for the United States Department of Energy under contract DE-AC04-94AL85000.

1. General

Carbon and alloy steels can be categorized by a variety of characteristics such as composition, microstructure, strength level, material processing, and heat treatment [1]. The carbon and alloy steel categories selected for the Technical Reference for Hydrogen Compatibility of Materials were based on characteristics of the steels as well as available data. In this chapter, the steels are distinguished by the primary alloying elements, i.e., nickel (< 5.5 wt%), chromium (< 2.0 wt%), and molybdenum (< 0.75 wt%). Additionally, data in this chapter pertain to steels that were heat treated by heating in the austenite phase field (austenitizing), rapidly cooling (quenching) to form martensite, then tempering at intermediate temperatures to achieve the final mechanical properties. Hydrogen compatibility data exist primarily for the following Ni-Cr-Mo steels: 4340, HY-80, HY-100, HY-130, and A517 (F). Since a full range of data is not available for each steel, data for all Ni-Cr-Mo steels are presented in this chapter. Although the steels exhibit some metallurgical differences, many of the data trends are expected to apply to each steel.

The Ni-Cr-Mo steels are attractive structural materials in applications such as pressure vessels because of combinations of strength and toughness that can be achieved through quenching and tempering. However, the quenched and tempered Ni-Cr-Mo steels must be used judiciously in structures exposed to hydrogen gas. Hydrogen gas degrades the strength and ductility of Ni-Cr-Mo steels, particularly in the presence of stress concentrations. Additionally, hydrogen gas lowers fracture toughness and renders the steels susceptible to crack extension under static loading. Hydrogen gas also accelerates fatigue crack growth. The severity of these manifestations of hydrogen embrittlement depends on mechanical, material, and environmental variables. Important variables include loading rate, yield strength, steel composition, hydrogen gas pressure, and temperature. Control over these variables individually or in combination may allow Ni-Cr-Mo steels to be applied safely in hydrogen gas environments. For example, limiting steel yield strength and tailoring concentrations of manganese and silicon can improve resistance to hydrogen embrittlement.

This chapter emphasizes fracture mechanics properties, since pressure vessel design codes employ defect-tolerant design principles, particularly for hydrogen environments. Most fracture mechanics data for Ni-Cr-Mo steels have been generated for material and environmental conditions that do not reflect conditions anticipated for applications in a hydrogen energy infrastructure. For example, much of the data pertains to high-strength steels exposed to low hydrogen gas pressures. This chapter reports general data trends that must be considered for all Ni-Cr-Mo steels exposed to hydrogen gas, but much of the data is not intended for use in calculating design margins. Additional materials testing is needed to assure that hydrogen compatibility data are obtained for the specific combination of mechanical, material, and environmental variables required in any given application.

1.1. Composition, heat treatment, and mechanical properties

Table 1.1.1 lists the allowable composition ranges for Ni-Cr-Mo steels covered in this chapter. Table 1.1.2 summarizes the compositions of steels from hydrogen compatibility studies reported in this chapter. Table 1.1.3 details the heat treatments applied to steels in Table 1.1.2. Additionally, Table 1.1.3 includes the yield strength, ultimate tensile strength, reduction of area, and fracture toughness that result from the heat treatments.

1.2. Steel common names and selected specifications

4340: UNS G43400, AISI 4340, AMS 6415, ASTM A29 (4340), SAE J404 (4340)
HY-80: UNS K31820, MIL-S-23009 (HY80), ASTM A372 (K)
HY-100: UNS K32045, MIL-S-23009 (HY100)
HY-130: MIL-S-24512
A517 (F), T-1: UNS K11567, ASTM A517 (F)

2. Permeability

The permeability of annealed A517 (F) to low-pressure hydrogen gas was measured over the temperature range 260 to 700 K [2]. The annealed microstructure consisted of ferrite + pearlite rather than tempered martensite. The composition of the A517 (F) steel was not provided. The temperature dependence of permeability (ϕ) was reported as [2]:

$$\phi = 1.5\text{x}10^{-4}\ \frac{\text{mol H}_2}{\text{m}\cdot\text{s}\cdot\sqrt{\text{MPa}}}\exp\left(\frac{-39.3\ \frac{\text{kJ}}{\text{mol}}}{RT}\right)$$

3. Mechanical Properties: Effects of Gaseous Hydrogen

3.1. Tensile properties

3.1.1. Smooth tensile properties

Measurements from smooth tensile specimens of several Ni-Cr-Mo steels in high-pressure hydrogen gas demonstrate that hydrogen degrades reduction of area but not ultimate tensile strength. Table 3.1.1.1 shows that reduction of area values measured in high-pressure hydrogen gas are 15% lower compared to values measured in high-pressure helium gas for both HY-100 and HY-80 [3]. The reduction of area for A517 (F) is approximately the same in air and hydrogen gas; however, comparison of properties measured in high-pressure hydrogen gas to properties measured in air must account for the effect of hydrostatic pressure on reduction of area, yield strength, and tensile strength [3].[1] The lower tensile strengths for HY-80 and A517 (F) in hydrogen gas compared to values in air result from the effect of hydrostatic pressure.

The reduction of area measured in high-pressure hydrogen gas is sensitive to tensile specimen surface condition. Tensile data in Table 3.1.1.2 reflect an attempt to study the role of surface oxides on tensile fracture in high-pressure hydrogen gas [3]. The surfaces of smooth specimens from A517 (F) steel were abraded with a tool to expose fresh metal, then the specimens were tested in tension. The abrasion and testing procedures were conducted in different combinations of environments. The results in Table 3.1.1.2 show that abrasion followed by testing in hydrogen gas decreases the reduction of area for all abrasion environments and elapsed times after abrasion. The reduction of area measured in hydrogen gas was governed by the presence of surface grooves and irregularities produced by the abrading tool. The reduction of area measured

[1] Hydrostatic pressure imposed by high-pressure gas can reduce the yield and tensile strengths and increase the elongation and reduction of area of metals. Mild changes in tensile properties measured in high-pressure hydrogen gas compared to those measured in air may result from the effect of hydrostatic pressure on material deformation and not an environmental effect of hydrogen.

in hydrogen gas 2 days following abrasion (RA = 46%) was higher than the reduction of area measured 0.5 hr following abrasion (RA = 39%), suggesting that surface oxides reformed in the former case and increased the ductility. But the dominant effect of abrasion was to produce fine surface discontinuities that degraded the reduction of area in hydrogen gas.

3.1.2. Notched tensile properties

The reduction of area and tensile strength of Ni-Cr-Mo steels are more severely affected by hydrogen when measured from notched tensile specimens compared to smooth tensile specimens. Table 3.1.2.1 shows that reduction of area values measured from notched specimens in high-pressure hydrogen gas are 50 to 60% lower compared to values measured in high-pressure helium gas for HY-100 and HY-80 [3]. In addition, hydrogen gas degrades the reduction of area for A517 (F) by 70% compared to the value in air. The decrease in reduction of area for A517 (F) in hydrogen gas is likely to be more severe when accounting for the effect of hydrostatic pressure. The tensile strengths of HY-100, HY-80, and A517 (F) are lower by 20 to 30% in high-pressure hydrogen gas compared to values in high-pressure helium gas (Table 3.1.2.1) [3].

Variation in notch acuity does not significantly affect reduction of area and tensile strength in high-pressure hydrogen gas, as illustrated for A517 (F) steel in Table 3.1.2.2 [3]. Hydrogen reduces tensile strength compared to values in helium by approximately the same magnitude (20 to 25%) for specimens with stress concentration factors of 3.8, 5.8, and 8.4. Additionally, reduction of area in hydrogen is lower by 70 to 80% compared to values in air for all stress concentration factors.

3.2. Fracture mechanics

3.2.1. Fracture toughness

The fracture toughness in hydrogen gas (K_{IH}) strongly depends on loading rate. Figure 3.2.1.1 shows K_{IH} data that were produced for 4340 in low-pressure hydrogen gas using standardized procedures [4, 5]. The K_{IH} decreases by a factor of two as loading rate decreases over three orders of magnitude. For each loading rate, K_{IH} is less than the fracture toughness, K_{Ic} (Table 1.1.3).

3.2.2. Threshold stress-intensity factor

The critical stress-intensity factor for hydrogen-assisted crack extension under static loading is termed a threshold (i.e., K_{TH}). Values of K_{TH} are sensitive to material and environmental variables. The trends in K_{TH} as a function of these variables are described below.

<u>Effect of yield strength</u>

Yield strength is a critical material variable governing K_{TH}. The consistent trend is that K_{TH} decreases as yield strength increases [6-10]. The effect of yield strength can be quite dramatic, as demonstrated in Figure 3.2.2.1 for three 4340 steels tested in low-pressure (0.11 MPa) hydrogen gas [6]. The K_{TH} values decrease by a factor of four to eight for the different steels as yield strength increases in the range 1145 to 1875 MPa. The higher K_{TH} for steel B7 compared to steels B6 and B2 is attributed to effects of steel composition, but yield strength still governs K_{TH} in steel B7.

The dominant effect of yield strength is also observed for steels tested in high-pressure hydrogen gas [10]. Table 3.2.2.1 summarizes K_{TH} values for HY-80, A517 (F), and HY-130 in high-pressure (21 to 97 MPa) hydrogen gas. For constant gas pressure, K_{TH} consistently decreases as steel yield strength increases in the range 585 to 940 MPa.

Effect of steel composition

The segregation of impurity elements to grain boundaries facilitates hydrogen-assisted intergranular fracture and lowers K_{TH}. The impurity elements and heat treatment practices that promote temper embrittlement in alloy steels also exacerbate hydrogen-assisted fracture [11].

The common alloying elements manganese and silicon influence the tendency for impurity elements to segregate to grain boundaries. The segregated impurity elements act in concert with hydrogen to cause intergranular fracture, but the bulk concentrations of manganese and silicon govern K_{TH} [6]. The dominant effects of manganese and silicon on K_{TH} are illustrated in Figures 3.2.2.2 and 3.2.2.3 [6, 12]. In Figure 3.2.2.2, K_{TH} values for steels based on 4340 are plotted *vs* the sum of bulk manganese, silicon, sulfur, and phosphorus concentrations. Examination of the steel compositions associated with individual data points in Figure 3.2.2.2 reveals that K_{TH} is most sensitive to manganese and silicon. Values of K_{TH} measured in low-pressure hydrogen gas decrease by a factor of five as manganese and silicon increase, then K_{TH} reaches a lower limiting value. Low bulk concentrations of sulfur and phosphorus are not sufficient for increasing K_{TH}. In Figure 3.2.2.3, results for HY-130 in low-pressure hydrogen gas show that steel A with low manganese and silicon has consistently higher K_{TH} than steel F.

The dominant effects of bulk manganese and silicon concentrations and secondary roles of bulk sulfur and phosphorus concentrations are supported by results from Sandoz [7, 13]. In this study, the concentrations of chromium, molybdenum, manganese, cobalt, carbon, sulfur, and phosphorus were individually varied in steels based on 4340. Tests in low-pressure hydrogen gas demonstrated that increases in manganese from 0.07 to 2.65 wt% decreased K_{TH} (Figure 3.2.2.4). In contrast, increases in sulfur and phosphorus concentrations in the range 0.002 to 0.027 wt% did not affect K_{TH}. Other results showed that variations in chromium and molybdenum did not affect K_{TH}. Variations in carbon had no effect on K_{TH} except at concentrations (i.e., 0.53 wt%) above the composition limit for 4340, where K_{TH} increased.

A notable result from the Sandoz study [7, 13] is that elements not included in the 4340 steel specification (Table 1.1.1) can improve K_{TH}. As cobalt was added to 4340 in concentrations from 0.39 to 2.83 wt%, K_{TH} was increased by 50% (Figure 3.2.2.4).

Effect of thermal aging

Aging in the tempering temperature window for extended times can lower K_{TH}. The effects of extended aging following quenching and tempering are demonstrated for two HY-130 steels in low-pressure hydrogen gas (Figure 3.2.2.3) [12]. Both steels suffer a sharp decline in K_{TH} after 50 hours of aging. In particular, K_{TH} for the steel with high manganese and silicon (steel F) decreases by a factor of two. As aging time increases up to 1000 hours, K_{TH} continues to decrease for both steels. The decrease in K_{TH} as a function of aging time has been attributed to the thermally activated process of impurity segregation [14]. As described in the previous

section, impurities that segregate to grain boundaries act in concert with hydrogen to promote intergranular fracture and lower K_{TH}.

Effect of austenitizing temperature
Limited data suggest that austenitizing temperature does not significantly affect K_{TH} (Figure 3.2.2.5) [15]. In the study represented in Figure 3.2.2.5, increasing the austenitizing temperature increased the prior austenite grain size but did not significantly alter the amount of retained austenite or the yield strength after tempering. The K_{TH} values were defined at a crack growth rate of approximately $7x10^{-4}$ mm/s from experiments in low-pressure hydrogen gas. Because of scatter in crack growth rate data [15] and low absolute values of K_{TH}, it is difficult to make firm conclusions from the data.

Effect of gas pressure
Hydrogen gas pressure is a critical environmental variable governing K_{TH}. The prevailing trend is that K_{TH} decreases as gas pressure increases [6, 9, 10, 16, 17]. The K_{TH} *vs* gas pressure trends are influenced by other environmental and material variables such as temperature and yield strength. The K_{TH} *vs* gas pressure plots constructed for 4340 steel (1070 MPa yield strength) at three temperatures in Figure 3.2.2.6 [9] are typical for Ni-Cr-Mo steels. The plots for the two higher temperatures show that K_{TH} decreases and approaches a lower limiting value as gas pressure increases. The plots are shifted to higher K_{TH} values as temperature increases.

Results do not reveal a consistent effect of yield strength on the relationship between K_{TH} and gas pressure. Data indicate that K_{TH} for high-strength 4340 approaches a lower limiting value at relatively low gas pressures [6, 16, 17], as illustrated in Figure 3.2.2.7. In contrast, K_{TH} for the lower-strength steel HY-130 (940 MPa yield strength) is still affected by gas pressure in the range 21 to 97 MPa (Table 3.2.2.1) [10]. These sets of data suggest that K_{TH} in lower-strength Ni-Cr-Mo steels does not approach a lower limiting value until much higher gas pressures. However, K_{TH} values for lower-strength A517 (F) (760 MPa yield strength) do not vary as a function of gas pressure between 21 MPa and 97 MPa (Table 3.2.2.1) [10]. Despite the uncertain effect of yield strength on the relationship between K_{TH} and gas pressure, it must be emphasized that absolute values of K_{TH} decrease as yield strength increases for all gas pressure ranges as described previously.

Effect of temperature
The K_{TH} can increase markedly as temperature increases above ambient [9, 16, 18]. The K_{TH} *vs* temperature data in Figure 3.2.2.8 for 4340 in low-pressure hydrogen gas show that absolute temperatures only 75 K above ambient increase K_{TH} by a factor of three, while absolute temperatures 65 K below ambient do not affect K_{TH} [16]. A similar effect of elevated temperature on K_{TH} is observed in Figure 3.2.2.6 [9].

3.3. Fatigue

3.3.1. Low-cycle fatigue
Hydrogen did not affect the low-cycle fatigue strength of A517 (F) [3]. Two smooth tensile specimens were each subjected to 3000 load cycles in 69 MPa hydrogen gas and did not exhibit

failure. The specimens were cycled over a stress range from 20 to 780 MPa at a frequency of 0.14 Hz.

3.3.2. Fatigue crack propagation

Hydrogen gas enhances the fatigue crack growth rate (da/dN) [17, 19]. The effect of high-pressure hydrogen gas on the crack growth rate *vs* stress-intensity factor range (ΔK) relationship for HY-100 steel is demonstrated in Figure 3.3.2.1 [17]. The crack growth rates in hydrogen gas exceed those in helium gas at all ΔK levels. The ratio of crack growth rates in hydrogen and helium environments becomes more pronounced as ΔK increases and reaches a value of about 20 at the highest ΔK levels.

Fatigue crack growth rates increase as hydrogen gas pressure increases, as illustrated for HY-100 in Figure 3.3.2.2 [17]. The data show that da/dN (at fixed $\Delta K = 55$ MPa$\sqrt{m}$) increases continuously as gas pressure increases.

Hydrogen can accelerate fatigue crack growth in lower-strength steels more than higher-strength steels [19]. Fatigue crack growth measurements in low-pressure hydrogen gas show that crack growth rates are higher in HY-80 compared to HY-130 (Figure 3.3.2.3). At higher ΔK levels, da/dN in HY-80 exceeds da/dN in HY-130 by a factor of 10. Crack growth rates in air are similar for the HY-80 and HY-130 steels. The effect of yield strength on fatigue crack growth indicated in Figure 3.3.2.3 is opposite to the effect of yield strength on K_{TH} (e.g., Figure 3.2.2.1).

3.4. Creep

No known published data in hydrogen gas.

3.5. Impact

No known published data in hydrogen gas.

4. Fabrication

4.1. Properties of welds

The hydrogen compatibility of the heat-affected zone and fusion zone of welds must be considered. Performance of welds should not be gauged based on data for base metal.

5. References

1. "Classification and Designation of Carbon and Low-Alloy Steels", in *Metals Handbook, Properties and Selection: Irons, Steels, and High-Performance Alloys*, 10th ed., vol. 1, ASM International, Materials Park OH, 1990, pp. 140-194.
2. MR Louthan, RG Derrick, JA Donovan, and GR Caskey, "Hydrogen Transport in Iron and Steel", in *Effect of Hydrogen on Behavior of Materials*, AW Thompson and IM Bernstein, eds., The American Institute of Mining, Metallurgical, and Petroleum Engineers, New York NY, 1976, pp. 337-347.
3. RJ Walter and WT Chandler, "Effects of High-Pressure Hydrogen on Metals in Ambient Temperatures Final Report," R-7780-1 (NASA contract NAS8-14), Rocketdyne, Canoga Park CA, 1969.

4. WG Clark and JD Landes, "An Evaluation of Rising Load K_{Iscc} Testing", in *Stress Corrosion - New Approaches, ASTM STP 610*, ASTM, Philadelphia PA, 1976, pp. 108-127.
5. "Standard Test Method for Measurement of Fracture Toughness," Standard E 1820-01, ASTM International, West Conshohocken PA, 2002.
6. N Bandyopadhyay, J Kameda, and CJ McMahon, "Hydrogen-Induced Cracking in 4340-Type Steel: Effects of Composition, Yield Strength, and H_2 Pressure", *Metallurgical Transactions A*, vol. 14A, 1983, pp. 881-888.
7. G Sandoz, "A Unified Theory for Some Effects of Hydrogen Source, Alloying Elements, and Potential on Crack Growth in Martensitic AISI 4340 Steel", *Metallurgical Transactions*, vol. 3, 1972, pp. 1169-1176.
8. S Hinotani, F Terasaki, and K Takahashi, "Hydrogen Embrittlement of High Strength Steels in High Pressure Hydrogen Gas at Ambient Temperature", *Tetsu-To-Hagane*, vol. 64, 1978, pp. 899-905.
9. GC Story, "Hydrogen Assisted Cracking of a Low Alloy Steel - Pressure, Temperature and Yield Strength Effects on the Threshold Fracture Toughness", PhD dissertation, University of California-Davis, Davis CA, 1980.
10. AW Loginow and EH Phelps, "Steels for Seamless Hydrogen Pressure Vessels", *Corrosion*, vol. 31, 1975, pp. 404-412.
11. CJ McMahon, "Hydrogen-Induced Intergranular Fracture of Steels", *Engineering Fracture Mechanics*, vol. 68, 2001, pp. 773-788.
12. Y Takeda and CJ McMahon, "Strain Controlled vs Stress Controlled Hydrogen Induced Fracture in a Quenched and Tempered Steel", *Metallurgical Transactions A*, vol. 12A, 1981, pp. 1255-1266.
13. G Sandoz, "The Effects of Alloying Elements on the Susceptibility to Stress-Corrosion Cracking of Martensitic Steels in Salt Water", *Metallurgical Transactions*, vol. 2, 1971, pp. 1055-1063.
14. CL Briant, HC Feng, and CJ McMahon, "Embrittlement of a 5 Pct Nickel High Strength Steel by Impurities and Their Effects on Hydrogen-Induced Cracking", *Metallurgical Transactions A*, vol. 9A, 1978, pp. 625-633.
15. M Nakamura and E Furubayashi, "Effect of Grain Size on Crack Propagation of High Strength Steel in Gaseous Hydrogen Atmosphere", *Materials Science and Technology*, vol. 6, 1990, pp. 604-610.
16. WG Clark, "Effect of Temperature and Pressure on Hydrogen Cracking in High Strength Type 4340 Steel", *Journal of Materials for Energy Systems*, vol. 1, 1979, pp. 33-40.
17. RJ Walter and WT Chandler, "Influence of Gaseous Hydrogen on Metals Final Report," NASA-CR-124410, NASA, Marshall Space Flight Center AL, 1973.
18. S Pyun and H Lie, "Relationship Between Hydrogen-Assisted Crack Propagation Rate and the Corresponding Crack Path in AISI 4340 Steel", *Steel Research*, vol. 61, 1990, pp. 419-425.
19. WG Clark, "The Effect of Hydrogen Gas on the Fatigue Crack Growth Rate Behavior of HY-80 and HY-130 Steels", in *Hydrogen in Metals*, IM Bernstein and AW Thompson, eds., ASM, Metals Park OH, 1974, pp. 149-164.
20. *Metals & Alloys in the Unified Numbering System*, Standard SAE HS-1086/2004, 10th ed., SAE International, Warrendale PA, 2004.

21. "Military Specification Steel Forgings, Alloy, Structural, High Yield Strength (HY-130)," Specification MIL-S-24512, 1975.

Table 1.1.1. Allowable composition ranges (wt%) for Ni-Cr-Mo steels.*

Steel	Specification	Ref.	Ni	Cr	Mo	C	Mn	Si	P	S	Other
4340	UNS G43400	[20]	1.65 2.00	0.70 0.90	0.20 0.30	0.38 0.43	0.60 0.80	0.15 0.30	0.035 max	0.040 max	-
HY-80	UNS K31820	[20]	2.00 3.25	1.00 1.80	0.20 0.60	0.18 max	0.10 0.40	0.15 0.35	0.015 max	0.008 max	0.25 max Cu 0.03 max V 0.02 max Ti
HY-100	UNS K32045	[20]	2.25 3.50	1.00 1.80	0.20 0.60	0.20 max	0.10 0.40	0.15 0.35	0.015 max	0.008 max	0.25 max Cu 0.03 max V 0.02 max Ti
HY-130	MIL-S-24512	[21]	4.75 5.25	0.40 0.70	0.30 0.65	0.12 max	0.60 0.90	0.20 0.35	0.010 max	0.010 max	0.25 max Cu 0.05<V<0.10 0.02 max Ti
A517 (F)	UNS K11567	[20]	0.70 1.00	0.40 0.65	0.40 0.60	0.10 0.20	0.60 1.00	0.15 0.35	0.035 max	0.040 max	0.15<Cu<0.50 0.03<V<0.08 0.0005<B<0.006

*The total weight percent of elements listed does not add up to 100%; the balance for each steel is Fe.

Table 1.1.2. Compositions (wt%) of Ni-Cr-Mo steels in hydrogen compatibility studies.*

Steel	Ref.	Ni	Cr	Mo	C	Mn	Si	P	S	Other
HY-100	[3]	2.57	1.67	0.42	0.16	0.32	0.22	0.010	0.019	0.05 Cu 0.002 V 0.001 Ti
HY-80	[3]	2.49	1.46	0.43	0.13	0.30	0.22	0.016	0.021	0.05 Al 0.002 V 0.001 Ti
A517 (F)	[3]	0.79	0.54	0.43	0.16	0.80	0.21	0.010	0.016	0.04 V 0.002 B
4340	[4, 16]	2.54	0.86	0.39	0.36	0.76	0.25	0.010	0.010	0.093 V
modified 4340 (steel B7)	[6]	1.82	0.81	0.25	0.37	0.007	0.002	0.003	0.003	0.002 Cu
4340 (steel B6)	[6]	1.80	0.75	0.26	0.37	0.72	0.32	0.003	0.005	-
4340 (steel B2)	[6]	1.72	0.73	0.22	0.39	0.68	0.08	0.009	0.016	0.046 Al 0.05 V 0.04 Nb
modified 4340 (steel 43Mn)	[7, 13]	1.82	0.75	0.30	0.24	0.07 2.65	0.27	0.003	0.01	-
modified 4340 (steel 43Co)	[7, 13]	1.74	0.85	0.26	0.30	0.79	0.32	0.001	0.004	0.39<Co<2.83
4340	[9]	1.75	0.79	0.26	0.41	0.76	0.28	0.008	0.004	0.14 Cu
HY-80	[10]	2.26	1.46	0.30	0.16	0.28	0.22	0.011	0.016	0.016 Al 0.005 V
A517 (F)	[10]	0.87	0.53	0.43	0.17	0.79	0.23	0.010	0.016	0.27 Cu 0.031 Al 0.039 V 0.003 B
HY-130	[10]	4.91	0.58	0.58	0.11	0.85	0.27	0.009	0.007	0.021 Al 0.05 V
HY-130 (steel A)	[12]	4.90	0.51	0.50	0.14	0.02	0.03	0.004	0.005	0.075 V 0.300 Al 0.002 N 0.0018 Sn
HY-130 (steel F)	[12]	4.97	0.48	0.50	0.13	0.90	0.36	0.004	0.006	0.079 V 0.025 Al 0.002 N 0.0009 Sn
4340	[15]	1.74	0.67	0.22	0.44	0.74	0.28	0.015	0.006	-
4340	[17]	1.81	0.82	0.22	0.39	0.63	0.27	0.008	0.017	-
HY-100	[17]	2.86	1.40	0.41	0.16	0.31	0.20	0.012	0.019	0.13Cu 0.003 Ti 0.003 V
HY-80	[19]	2.99	1.68	0.41	0.18	0.30	0.20	0.018	0.013	0.005 V
HY-130	[19]	4.96	0.57	0.41	0.12	0.79	0.35	0.004	0.005	0.057 V

*The total weight percent of elements listed does not add up to 100%; the balance for each steel is Fe.

Table 1.1.3. Heat treatments and mechanical properties of Ni-Cr-Mo steels in hydrogen compatibility studies.

Steel	Ref.	S_y (MPa)	S_u (MPa)	RA (%)	K_{Ic} (MPa√m)	Heat Treatment
HY-100	[3]	730	845	65	-	specification MIL-S-16216G
HY-80	[3]	620	735	69	-	specification MIL-S-16216G
A517 (F)	[3]	765	835	63	-	A 1158 K/30 min + WQ + T 936 K/60 min
4340	[4, 16]	1235	1340	46	154 176	A 1122 K/240 min + WQ + T 833 K/240 min + WQ
mod. 4340 (steel B7)	[6]	1200 1860	-	-	45 105	A 1123 K/60 min + OQ + (373 K < T < 798 K)/60 min
4340 (steel B6)	[6]	1160 1860	-	-	40 90	
4340 (steel B2)	[6]	1145 1875	-	-	45 105	
mod. 4340 (steel 43Mn)	[7, 13]	1165	1305	-	115*	A 1255 K + Q + DT 689 K/(60 min + 60 min)
mod. 4340 (steel 43Co)	[7, 13]	1275	1415	-	115*	A 1255 K + Q + (672 K < DT < 727 K)/(60 min + 60 min)
4340	[9]	1070	1190	52	-	A 1323 K/90 min + OQ + SR 473 K/60 min + WQ + TA 198 K/180 min + T 838 K/90 min + WQ
HY-80	[10]	585	690	77	125*	A 1177 K/90 min + WQ + T 997 K/90 min + WQ
A517 (F)	[10]	760	835	66	157*	A 1177 K/60 min + WQ + 938 K/90 min + WQ
HY-130	[10]	940	985	70	185*	A 1089 K/90 min + WQ + 900 K/90 min + WQ
HY-130 (steel A)	[12]	1040	-	-	-	A 1273 K/120 min + WQ + T 898 K/120 min + WQ
HY-130 (steel F)	[12]	1000	-	-	-	
4340	[15]	1550	2000	0 40	35 50*	(1123 K < A < 1523 K)/15 min + 1123 K/10 min + OQ + T 473 K/60 min
4340	[17]	1380	-	-	-	A 1089 K/60 min + OQ + T 644 K/120 min
HY-100	[17]	765	855	70	-	-
HY-80	[19]	655	780	70	-	A 1172 K + WQ + T 950 K + WQ
HY-130	[19]	965	1020	67	-	A 1089 K + WQ + T 866 K + WQ

A = austenitize; DT = double temper; OQ = oil quench; Q = quench; SR = stress relieve; T = temper; TA = transform austenite; WQ = water quench
*not reported as standardized K_{Ic} measurement

Table 3.1.1.1. Smooth tensile properties of Ni-Cr-Mo steels in air, high-pressure helium gas, and high-pressure hydrogen gas at room temperature.

Steel	Ref.	Test Environment	Strain Rate (s^{-1})	S_y (MPa)	S_u (MPa)	El_t (%)	RA (%)
HY-100	[3]	69 MPa He 69 MPa H_2	$3.3x10^{-5}$*	669† -	780 793	20‡ 18‡	76 63
HY-80	[3]	air 69 MPa He 69 MPa H_2	$3.3x10^{-5}$*	642† 566† 587†	738 676 683	- 23‡ 20‡	64 70 60
A517 (F)	[3]	air 69 MPa H_2	$3.3x10^{-5}$*	835† 745†	897 842	18‡ 18‡	67 65

*strain rate up to S_y
†defined at deviation from linearity on load *vs* time plot
‡based on 32 mm gauge length

Table 3.1.1.2. Smooth tensile properties of A517 (F) steel in air and high-pressure hydrogen gas at room temperature as a function of surface preparation.

Steel	Ref.	Abrading Environment	Time After Abrading Before H_2 Contact	Test Environment	Strain Rate* (s^{-1})	S_y† (MPa)	S_u (MPa)	El_t‡ (%)	RA (%)
A517 (F)	[3]	no abrasion		air	$3.3x10^{-5}$	835	897	18	67
		air	n/a	air		835	890	18	64
		no abrasion		69 MPa H_2		745	842	18	65
		air	0.5 hr	69 MPa H_2		766	856	12	39
		air	2 days	69 MPa H_2		731	835	14	46
		69 MPa H_2	n/a	69 MPa H_2		738	821	13	43

*strain rate up to S_y
†defined at deviation from linearity on load *vs* time plot
‡based on 32 mm gauge length

Table 3.1.2.1. Notched tensile properties of Ni-Cr-Mo steels in air, high-pressure helium gas and high-pressure hydrogen gas at room temperature.

Steel	Ref.	Specimen	Test Environment	Displacement Rate (mm/s)	S_y* (MPa)	σ_s (MPa)	RA (%)
HY-100	[3]	(a)	69 MPa He 69 MPa H_2	~ $4x10^{-4}$	669 -	1546 1132	7.3 3.8
HY-80	[3]	(a)	69 MPa He 69 MPa H_2	~ $4x10^{-4}$	566 587	1311 1069	8.6 3.6
A517 (F)	[3]	(a)	air 69 MPa He[a] 69 MPa H_2	~ $4x10^{-4}$	835 - 745	1628 1532[b] 1194	7.4 5.7 2.1

*yield strength of smooth tensile specimen (Table 3.1.1.1)
[a]contaminated with hydrogen
[b]estimated from strength measured in air and effect of hydrostatic pressure
(a) V-notched specimen: 60° included angle; minimum diameter = 3.81 mm; maximum diameter = 7.77 mm; notch root radius = 0.024 mm. Stress concentration factor (K_t) = 8.4.

Table 3.1.2.2. Notched tensile properties as a function of notch acuity for A517 (F) steel in air, high-pressure helium gas, and high-pressure hydrogen gas at room temperature.

Steel	Ref.	Specimen	Test Environment	Displacement Rate (mm/s)	σ_s (MPa)	RA (%)
A517 (F)	[3]	K_t = 3.8†	air 69 MPa He 69 MPa H_2	~ $4x10^{-4}$	1677 1566 1249	13 12 2.8
		K_t = 5.8†	air 69 MPa He 69 MPa H_2		1677 1587 1187	11 12 2.0
		K_t = 8.4†	air 69 MPa He[a] 69 MPa H_2		1628 1532[b] 1194	7.4 5.7 2.1

K_t = stress concentration factor
†V-notched specimen: 60° included angle; minimum diameter = 3.81 mm; maximum diameter = 7.77 mm; notch root radius = 0.117, 0.051, and 0.024 mm for K_t = 3.8, 5.8, and 8.4, respectively.
[a]contaminated with hydrogen
[b]estimated from strength measured in air and effect of hydrostatic pressure

Table 3.2.2.1. Values of threshold stress-intensity factor for Ni-Cr-Mo steels in high-pressure hydrogen gas at 286 K.

Steel	Ref.	$S_y^{\dagger}$ (MPa)	$RA^{\dagger}$ (%)	K_{Ic} (MPa√m)	Test Environment	K_{TH} (MPa√m)
HY-80	[10]	585	77	125*	69 MPa H_2 97 MPa H_2	NCP 116 NCP 89
A517 (F)	[10]	760	66	157*	21 MPa H_2 41 MPa H_2 62 MPa H_2 69 MPa H_2 97 MPa H_2	86 67 77 70 81
HY-130	[10]	940	70	185*	21 MPa H_2 41 MPa H_2 69 MPa H_2	36 32 24

NCP = no crack propagation at given stress intensity factor
†yield strength and reduction of area of smooth tensile specimen in air
*not reported as standardized K_{Ic} measurement

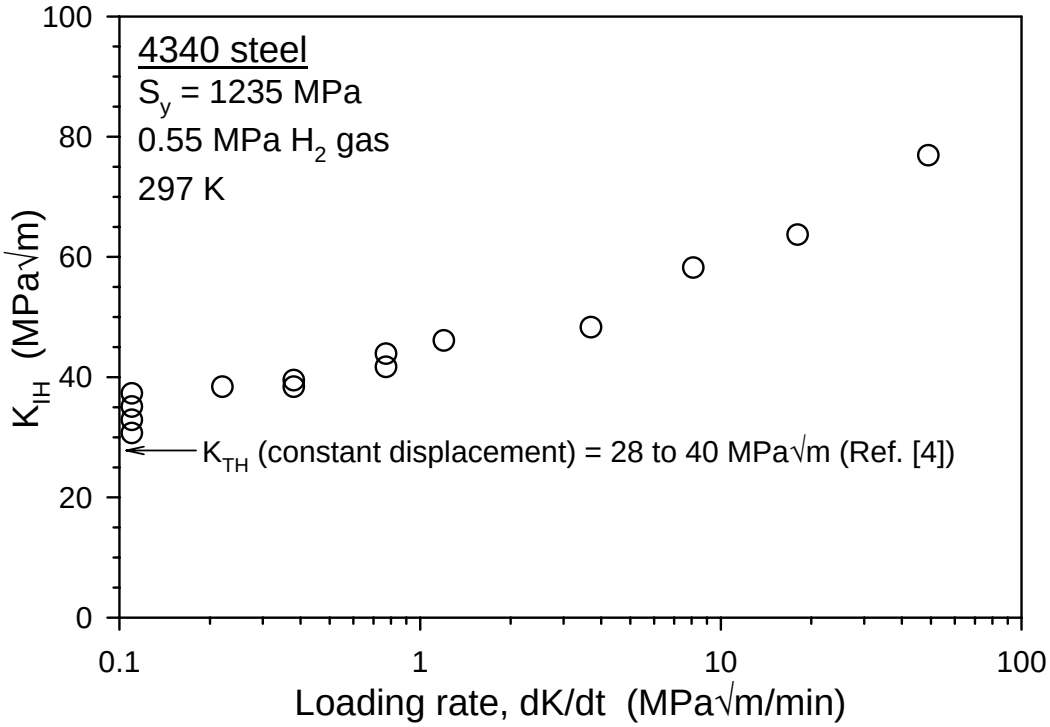

Figure 3.2.1.1. Effect of loading rate on fracture toughness in low-pressure hydrogen gas for 4340 steel [4].

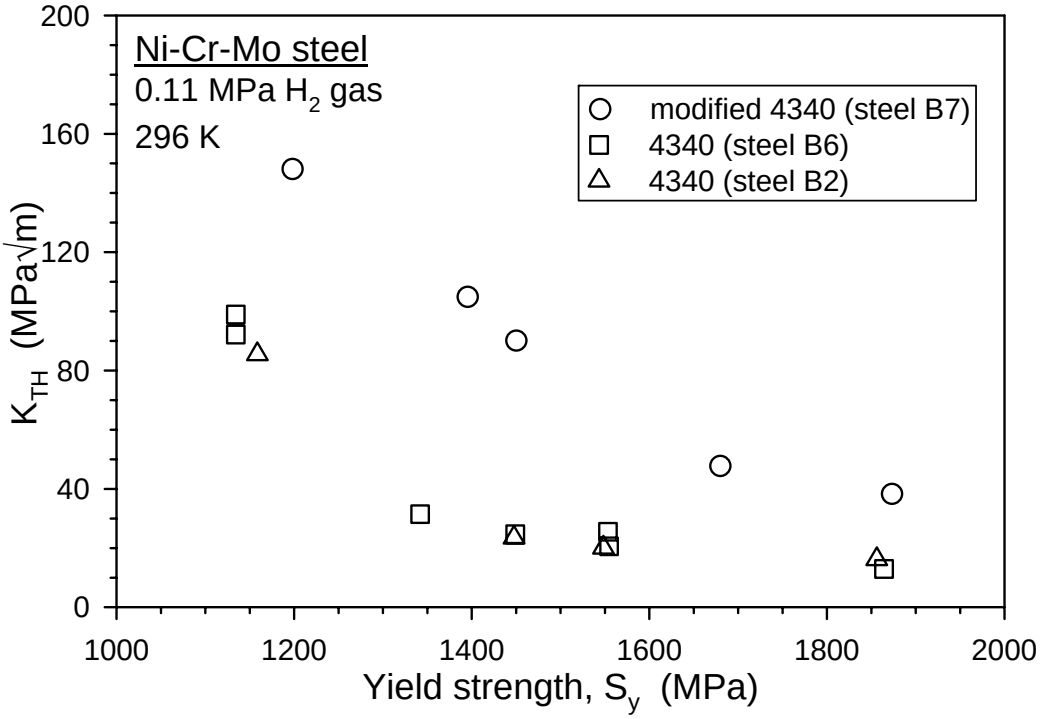

Figure 3.2.2.1. Effect of yield strength on threshold stress-intensity factor for crack extension in low-pressure hydrogen gas for steels based on 4340 [6].

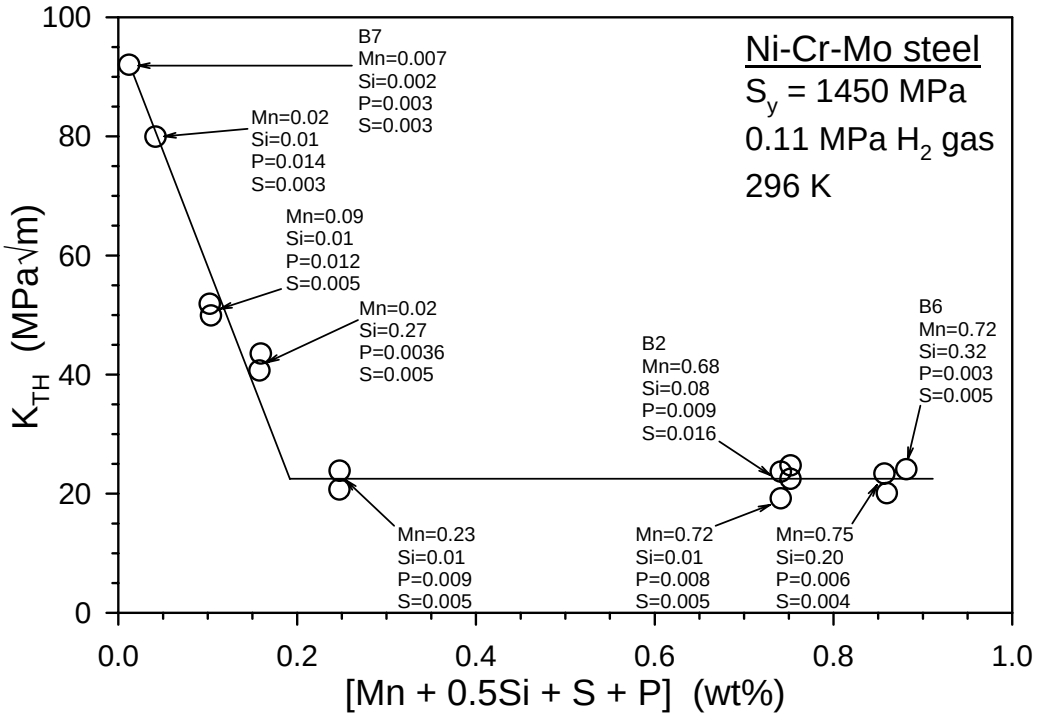

Figure 3.2.2.2. Effect of manganese, silicon, phosphorus, and sulfur content on threshold stress-intensity factor for crack extension in low-pressure hydrogen gas for steels based on 4340 [6].

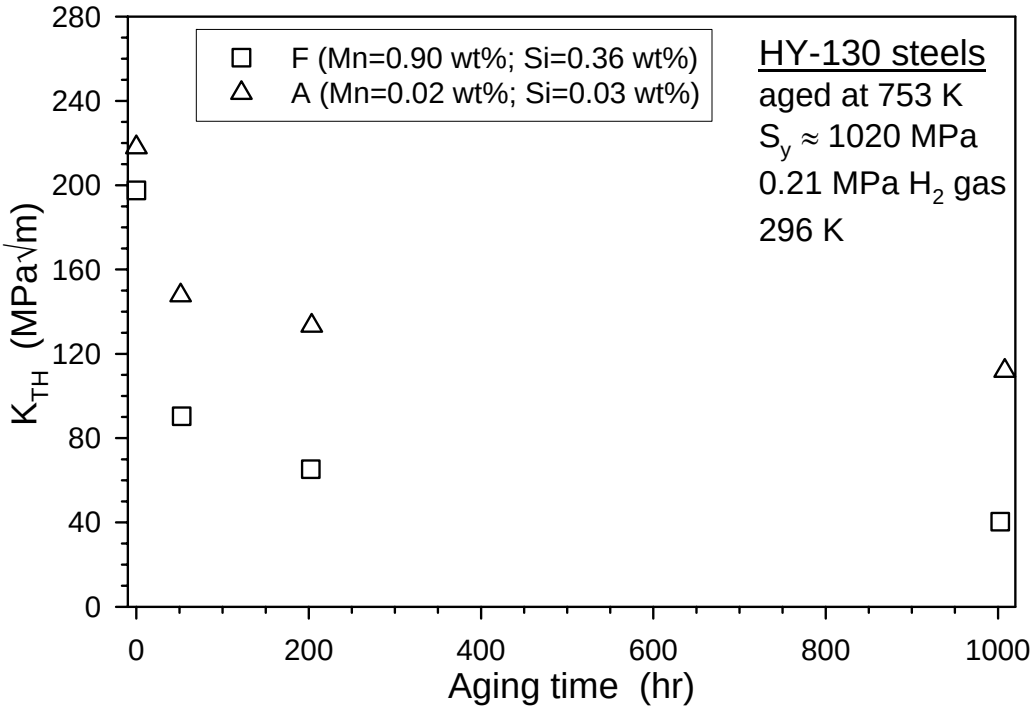

Figure 3.2.2.3 Effect of aging time at 753 K on the threshold stress-intensity factor for crack extension in low-pressure hydrogen gas for HY-130 steels [12].

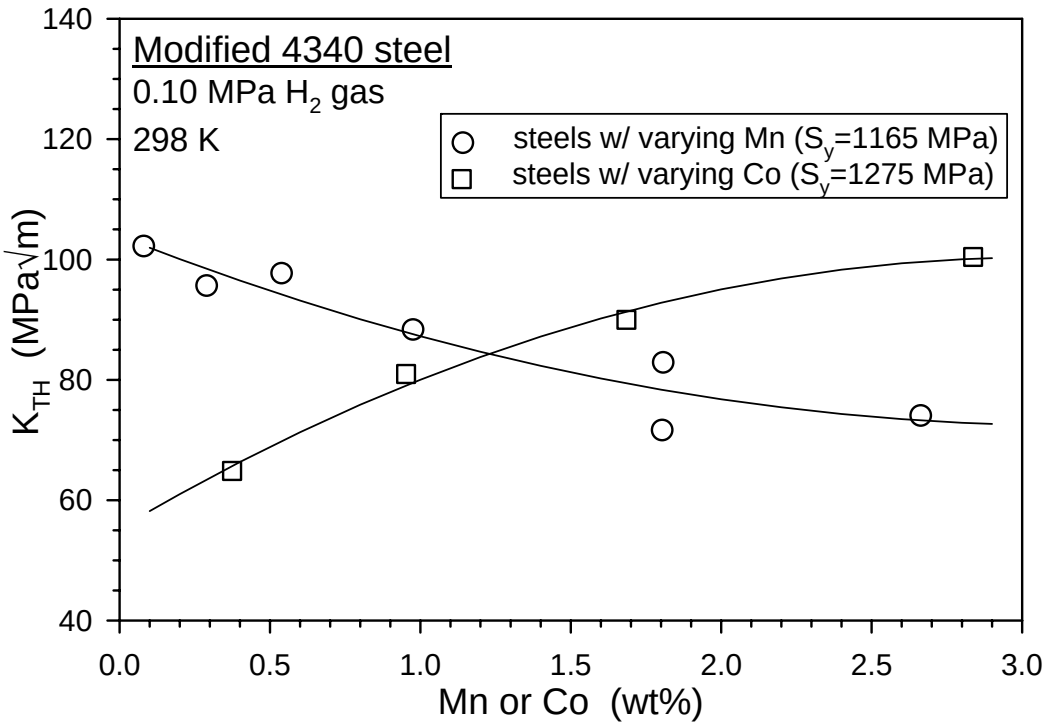

Figure 3.2.2.4. Effect of manganese or cobalt content on threshold stress-intensity factor for crack extension in low-pressure hydrogen gas for modified 4340 steels [7].

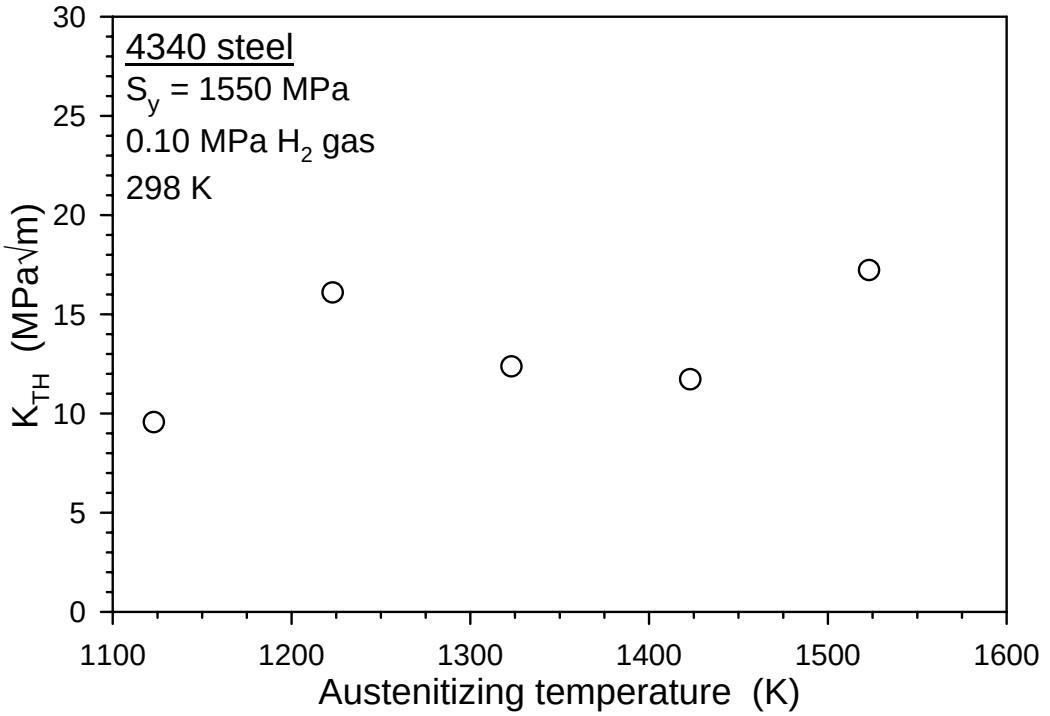

Figure 3.2.2.5. Effect of austenitizing temperature on threshold stress-intensity factor for crack extension in low-pressure hydrogen gas for 4340 steel [15].

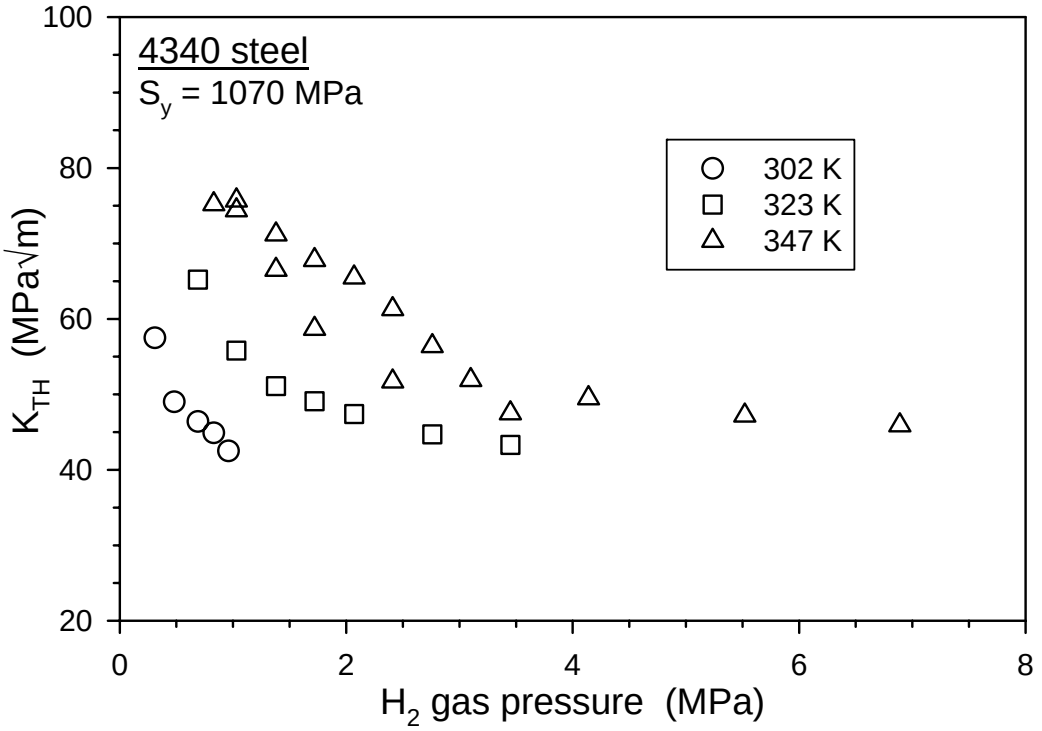

Figure 3.2.2.6. Effect of hydrogen gas pressure on threshold stress-intensity factor for crack extension in 4340 steel [9]. Data are shown for three temperatures.

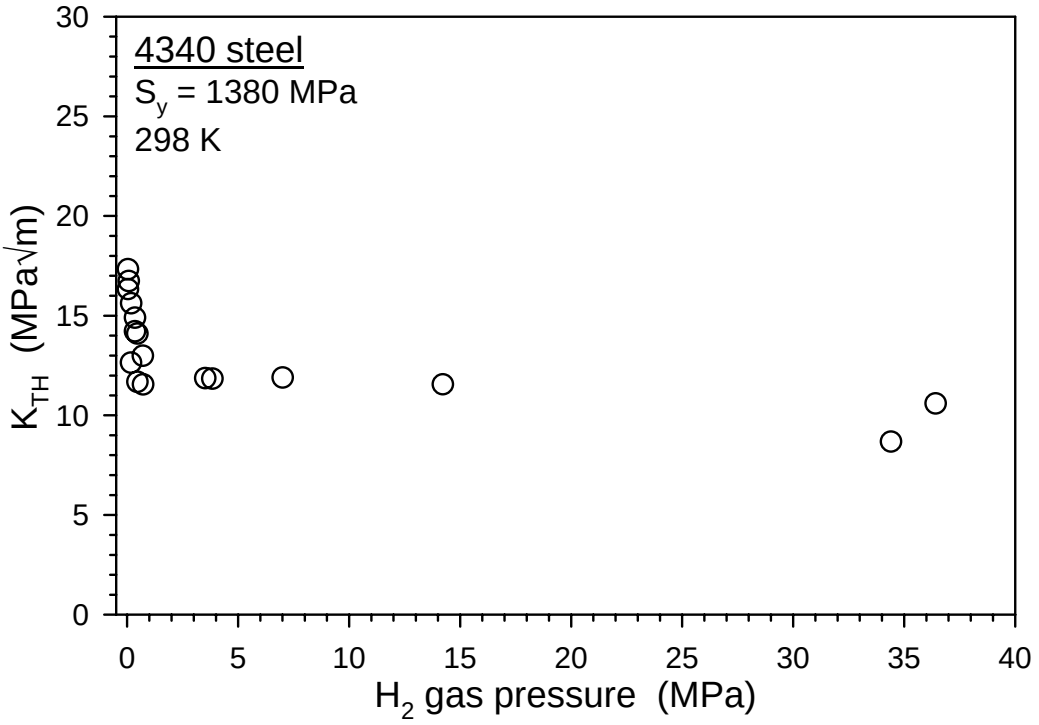

Figure 3.2.2.7. Effect of hydrogen gas pressure on threshold stress-intensity factor for crack extension in high-strength 4340 steel [17].

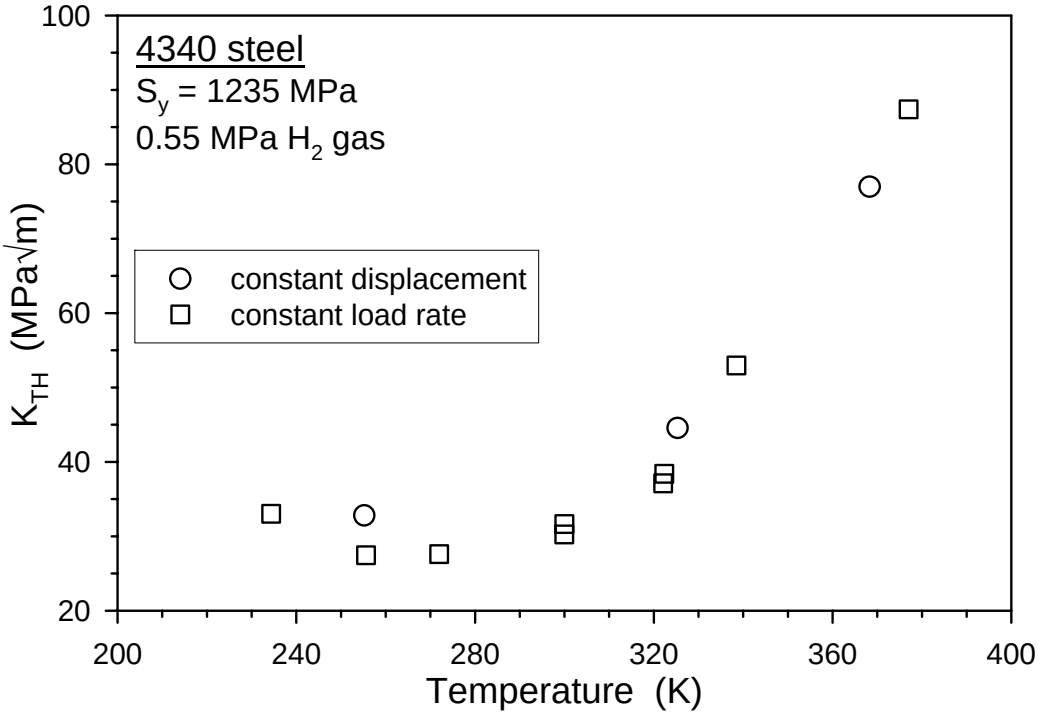

Figure 3.2.2.8. Effect of temperature on threshold stress-intensity factor for crack extension in low-pressure hydrogen gas for 4340 steel [16]. Two loading modes were used to generate the data: constant displacement and constant load rate (dK/dt = 0.1 to 0.2 MPa√m/min).

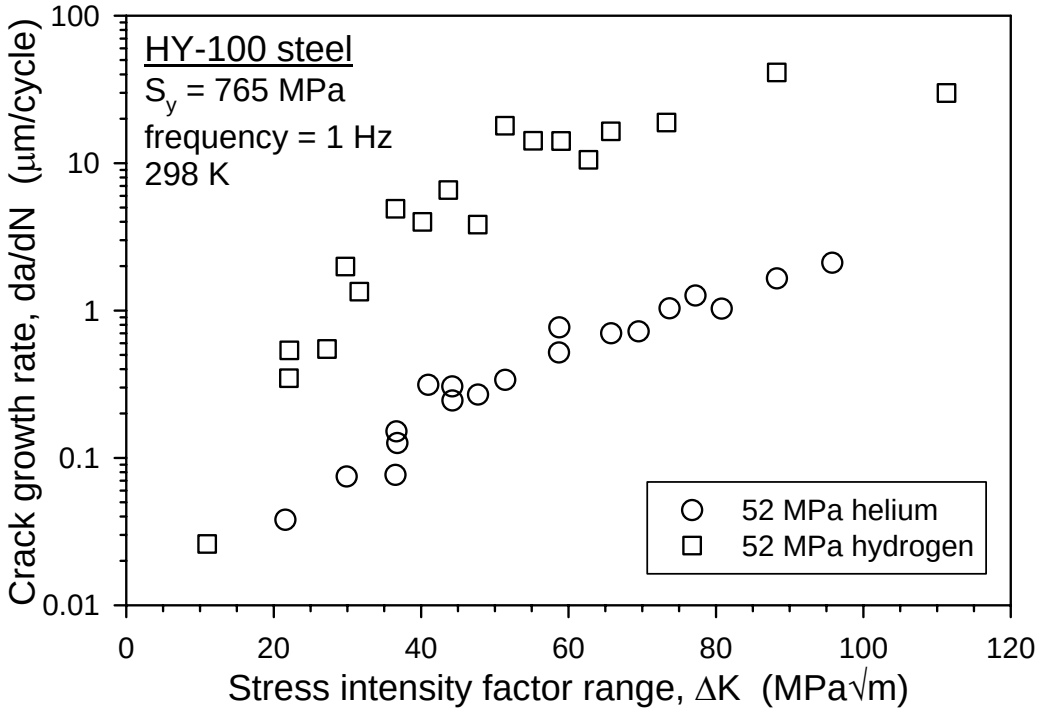

Figure 3.3.2.1. Fatigue crack growth rate as a function of stress-intensity factor range for HY-100 steel in high-pressure hydrogen and helium gases [17].

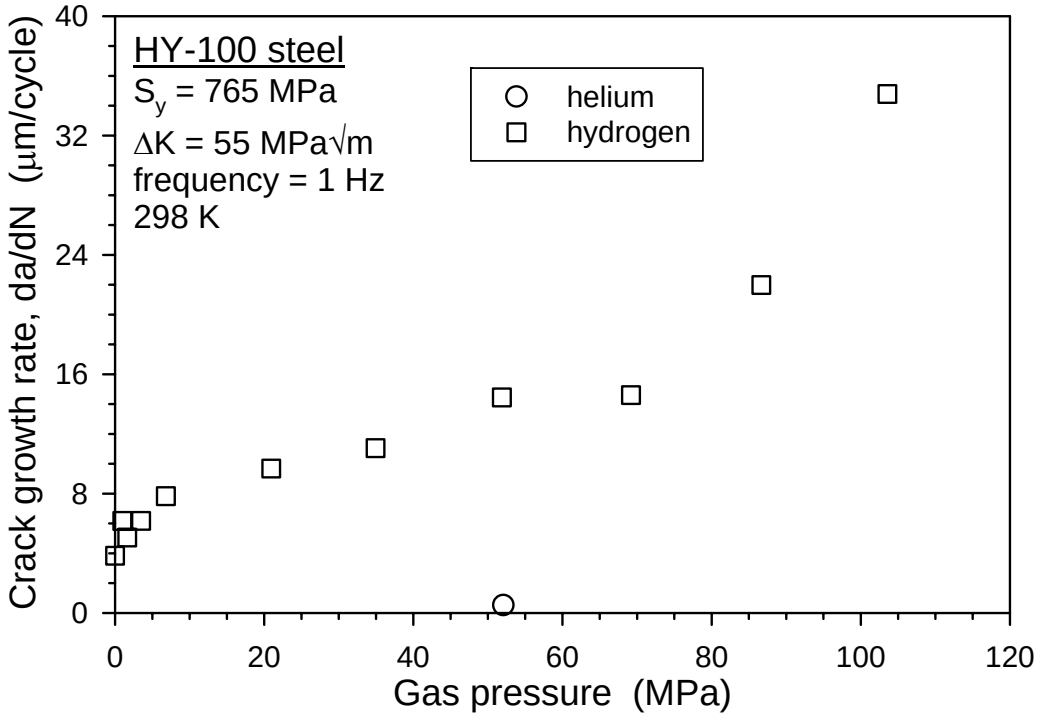

Figure 3.3.2.2. Fatigue crack growth rate as a function of hydrogen gas pressure for HY-100 steel at fixed stress-intensity factor range [17].

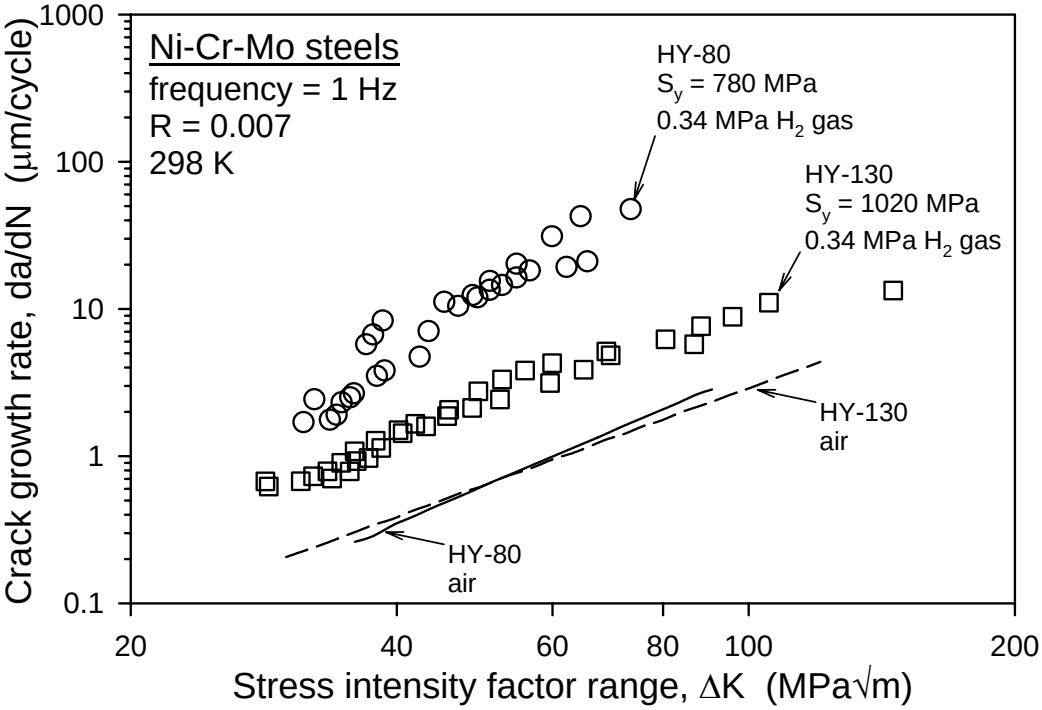

Figure 3.3.2.3. Fatigue crack growth rate as a function of stress-intensity factor range for HY-80 and HY-130 steels in air and low-pressure hydrogen gas [19].